



Deep drawability of additively manufactured sheets with a structured core

Stephan Rosenthal¹ · Marlon Hahn¹ · A. Erman Tekkaya¹

Received: 8 September 2022 / Accepted: 16 January 2023 / Published online: 14 February 2023
© The Author(s) 2023, corrected publication 2023

Abstract

The deep drawability of additively manufactured stainless steel sheets with a core structure is investigated. By fracture forming limit diagrams it is shown that the additively manufactured sheets reveal good formability. The deep drawing process is analyzed numerically and the numerical models are validated experimentally. The main failure mode is a fracture of the face sheets. No severe deformation of the core structure was encountered, leading to the fact that the parts keep their structural integrity after the deep drawing process. It is shown that the process forces can reasonably be predicted by a modified Siebel's method. A process window diagram is derived, e.g. showing a maximum deep drawing ratio $\beta_{\max} = 1.4$ for honeycomb structures with a relative core density of $\rho_{\text{core}} = 0.22$.

Keywords Deep drawing · Additive manufacturing · Sheet forming · Hybrid process · Laser-powderbed-fusion

Introduction and state of the art

Structured sheets with complex core structures offer a high structural and crash performance, high strength and good stiffness-to-weight ratio. This makes them a remarkable candidate for lightweight applications in aerospace, aviation, transportation as well as automobile applications. A method of manufacturing such sheets with complex core structures was proposed by Rosenthal et al. [1]. The idea is to use additive manufacturing (AM), specifically laser-powder-bed-fusion (L-PBF) of metals, for the production of flat semi-finished sheets with core structures, which are formed to the final geometry in a subsequent forming operation (Fig. 1). This not only leads to an increased structural performance of the parts due to strain hardening but also increases the overall process efficiency of the additive manufacturing process followed by post-processing steps up to 360% [1] compared to directly manufacturing the component in the final geometry.

Forming of sandwich structures with egg-box-like core structures was performed by Cai et al. [2]. In a numerical study, they used a multi-point forming die to investigate the

formability for the production of saddle-shaped parts. They discovered face sheet buckling as a main failure mechanism, which can be reduced by thickening the face sheet. In further experiments, Cai et al. [3] were able to form such structures with a thickness of 4 mm and 8.7 mm to radii of $R = 350$ mm and $R = 500$ mm. Further experimental work by Liang et al. [4] revealed that the formability of the structured sheets is dependent on the overall thickness as well as on the structure itself. Fine structures with thicknesses < 4 mm fail in buckling in a global manner, where the whole structure loses its shape under compressive stresses. Thick sheets (thickness $H = 4\text{--}10$ mm) fail as a result of intercellular buckling. Metallic sandwich sheets with sheared dimple cores and brazed face sheets with a limiting relative bending radius $R/H = 3.33$ were investigated by Seong et al. [5]. The main failure modes were delamination, core shear failure, face fracture, and face buckling [6]. Bending of additively manufactured sheets was investigated by Rosenthal et al. [1]. Sheets with honeycomb, spherical, and truss-like core structures were successfully formed to a hat-shaped profile with a bending ratio of $R/H = 2.5$, made from stainless steel 316 L. Though the forming of structured sheets with core structures was investigated to a certain degree so far, the next evolutionary step towards a complex deep drawing operation has not been done yet.

In this paper, deep drawing of cylindrical cups using additively manufactured semi-finished sheets with core

✉ Stephan Rosenthal

¹ Institute of Forming Technology and Lightweight Components (IUL), TU Dortmund University, 44227 Dortmund, Germany

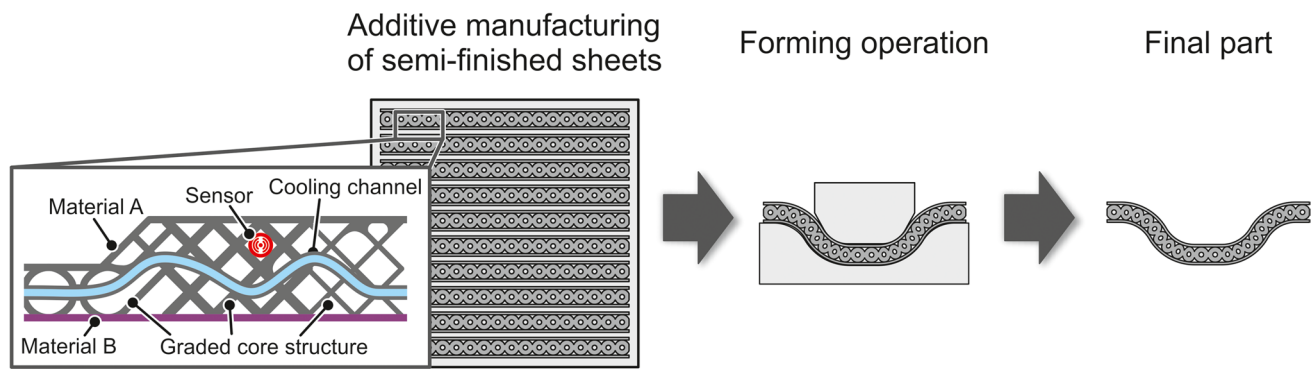


Fig. 1 Proposed process route. Additive manufacturing of semi-finished sheets with subsequent forming into the final geometry [1]

structures is investigated. The utilization of deep drawing beyond simple bending operations can further extend the applicability of these advanced semi-finished sheets with complex core structures, e.g. for lightweight applications.

Materials and methods

The used additively manufactured material SS 316 L is characterized and the forming limits are determined. Deep drawing is performed using semi-finished sheets having a honeycomb core structure. The manufacturing route and design of the components are presented. The deep drawing process is investigated employing numerical and experimental methods.

Material characterization

The powder used for the additive manufacturing in this study is stainless steel 316 L with a grain size distribution of 15–45 μm (Fig. 2a). The semi-finished sheets are manufactured on a DMG Mori Lasertec 30 SLM machine with a 600 W-laser and a build-chamber volume of $300 \times 300 \times 300 \text{ mm}^3$. The manufacturing directions of the specimen and the associated nomenclature is depicted in Fig. 2b.

The material behavior of the SS 316 L is shown in Fig. 3a. The tests are conducted using standard tensile tests in three manufacturing directions, 0°, 45°, and 90°-direction relative to the build platform (Fig. 3b). Flow curves at large strains are measured using the in-plane torsion test according to Traphöner et al. [7] with a grooved specimen (Fig. 3c). The true stress-strain curves show a slight anisotropic behavior with a directional yield stress ratio $\sigma_{y,0^\circ}/\sigma_{y,90^\circ} = 1.07$, where $\sigma_{y,0^\circ}$ and $\sigma_{y,90^\circ}$ stand for the initial yield stress in the manufacturing directions of the AM process. Hence, anisotropy may be neglected in further considerations.

The forming limits are determined as fracture forming limits (FFL) because the standard forming limits as described in the standard ISO 12004 [8] cannot be directly transferred to the novel semi-finished sheets. The challenge in this case is, that the structured sheets have an inhomogeneous material distribution and the face sheets are only partly connected to the core. For a final part, the load during the use is distributed over the core and the face sheets. It is assumed that a forming-induced necking of the face sheets is not critical. The core acts as a support that can absorb additional loads as long as the structural integrity of the overall part is still given. In the experimental investigation of the structured sheets, preliminary investigations by Rosenthal et al. [1] revealed that instead of necking, only actual fracture of the face sheets can accurately be recognized as

Fig. 2 a) Stainless steel 316 L powder for selective laser melting, b) Manufacturing direction of the AM specimen

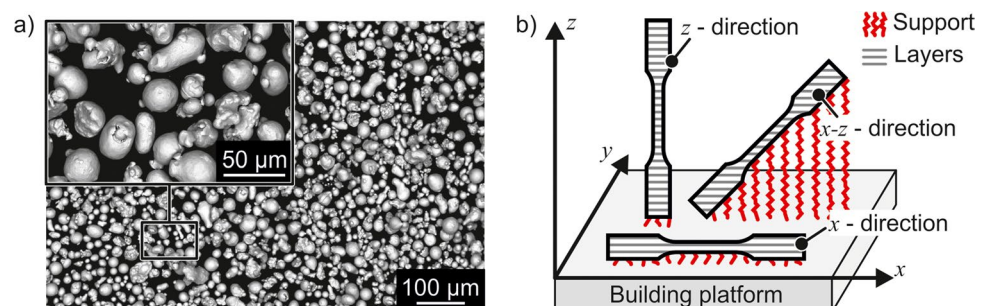
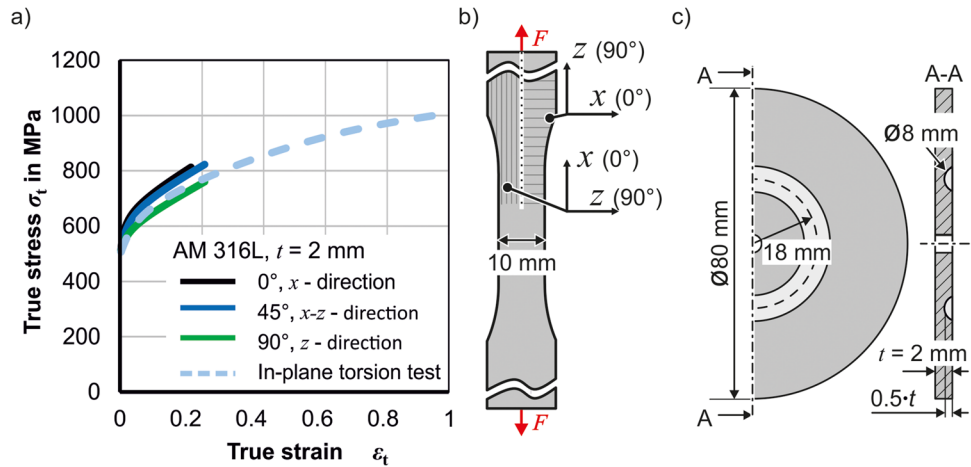


Fig. 3 Material characterization of SS 316 L, **a**) Flow curves, **b**) Tensile test specimen (manufacturing directions w.r.t Fig. 2b), **c**) In-plane torsion specimen



failure. Thus, it is suitable to use the fracture strain as a measure of formability in this case.

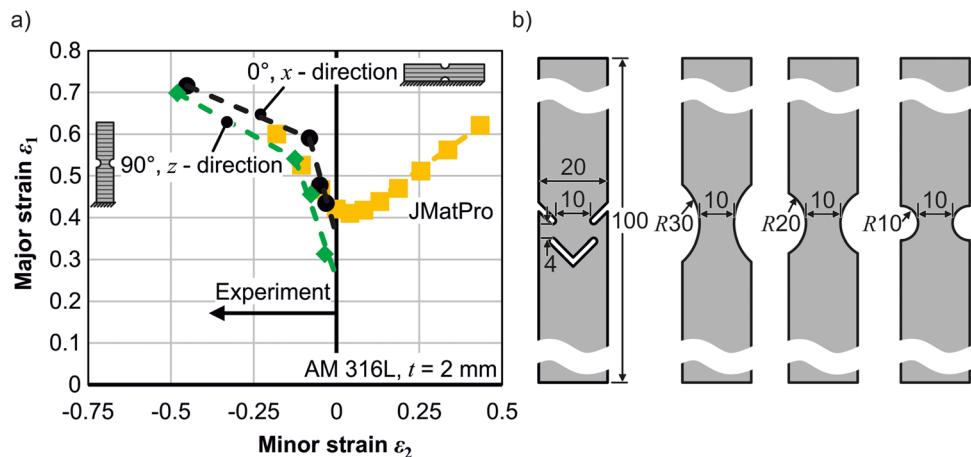
To characterize those failure strains, tensile tests with notched additively manufactured specimens as shown in Fig. 4b are performed, in order to achieve different ratios of major and minor logarithmic strains. The resulting fracture forming limit diagrams (FFL) are shown in Fig. 4a. The strains were measured with digital image correlation (DIC) using GOM Aramis 4 M system. The strain is evaluated at the DIC image just before the crack on the specimen starts to develop. The left-hand side ($\epsilon_1 > 0, \epsilon_2 < 0$) of the FFL can be determined with the presented specimen, the right-hand side ($\epsilon_1 > 0, \epsilon_2 > 0$) cannot be characterized with adjusted tensile test specimens but is also not crucial for the deep drawing of cylindrical cups. Therefore, these values are calculated using the CALPHAD (CALculation of PHase Diagrams) method [9] with the software JMatPro and calibrated to the experimental data, for the sake of completeness.

Semi-finished sheets

The semi-finished sheets which are used for the deep drawing process are shown in Fig. 5. The sheets consist of honeycomb unit cells (Fig. 5a), which are duplicated in the sheet-plane. To ensure the remaining powder from the AM-process can be removed, the core has built-in holes with a diameter of 1 mm. The length $l = 5.63$ mm, width $w = 3.25$ mm, core height $C = 3$ mm and face sheet thickness $t_f = 0.5$ mm are fixed across the variable relative densities $\rho_{core} = V_{UC}/V_{EQ}$ of the core. With V_{UC} as the actual volume of the unit cell and $V_{EQ} = l \cdot w \cdot C$ as the boundary volume of the core. To vary the relative density ρ_{core} of the core structure, the wall thickness d_H is changed.

The complete sheets with core structures in Fig. 5b incorporate about 3200 unit-cells and form a diameter of approximately 270 mm. The sheets are manufactured on specially designed support structures with a tapered cross section to ensure a stable manufacturing process. From the manufactured sheets, different diameters for the deep drawing experiments are cut out by a laser (Fig. 5c) to provide various

Fig. 4 Determination of forming limits of additively manufactured (AM) SS 316 L sheets, **a**) Fracture forming limit diagram (FFLD), **b**) Specimens to determine FFLD



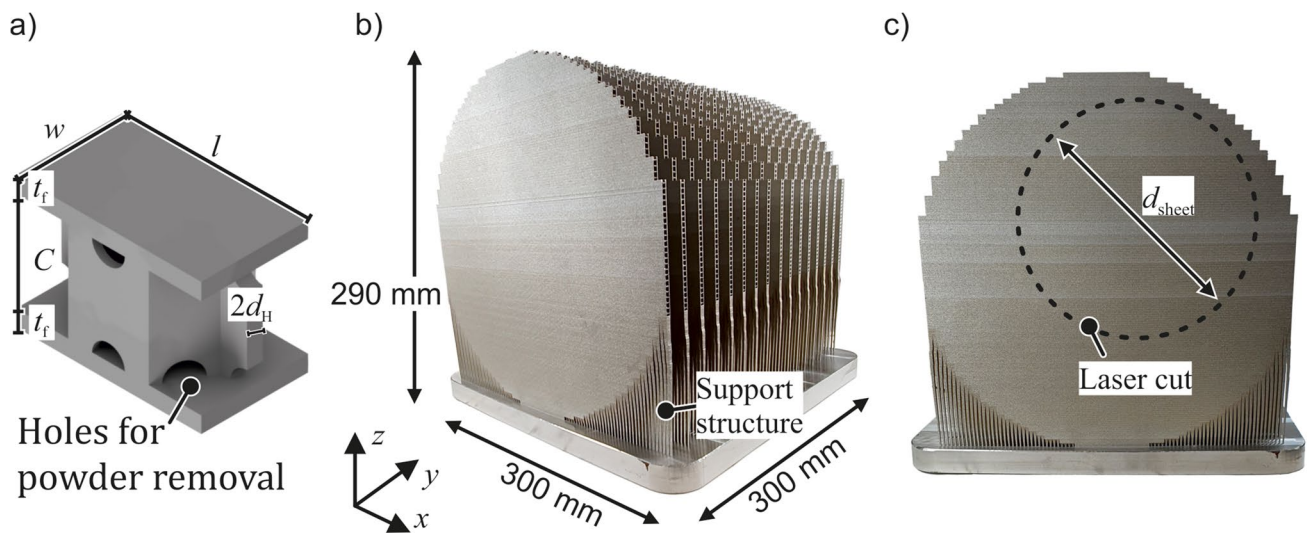


Fig. 5 a) Honeycomb unit cell, b) Additively manufactured sheets on the build platform, c) Front view of the sheets before post-processing and cutting

deep drawing ratios $\beta = d_{\text{sheet}}/d_{\text{tool}}$ (d_{sheet} : initial diameter of the deep drawn sheet; d_{tool} : diameter of the deep drawing punch).

The additive manufacturing process was performed using the standard process parameters provided by DMG Mori. The manufacturing time on the AM-machine for 18 sheets was ~ 900 h with an additional time of ~ 30 h for the post-processing of the sheets. The post-processing comprises the powder removal in the machine with a vacuum. Afterwards, the built platform was clamped onto a capsuled vibrating table to remove the powder from the inner cavities of the core structure, which is followed by a cleaning operation in a Joke ENESKA PostPro machine with pressured air and an ultrasonic cleaning bath. The sheets are removed from the platform by sawing.

Experimental and numerical investigations

Preliminary numerical investigations

Preliminary investigations regarding the deep drawability of additively manufactured sheets are necessary, since the novelty of the process route does not allow any conclusions to be drawn about existing process limits. Therefore, a rudimentary deep drawing process window is numerically predicted for a $t = 4$ mm thick solid sheet made of additively manufactured 316 L material. These information are used for a preselection of the investigated process parameters for the deep drawing of the sheets with a structured core. It is assumed, that the structured sheets have a lower maximum deep drawing ratio than a solid sheet from the same material.

The results of the numerical simulations are shown in Fig. 6. The equivalent strain distribution of the drawn cups show an axisymmetric strain distribution (Fig. 6a). The strains increase with increasing deep drawing ratio β . The maximum deep drawing ratio of the solid sheet is $\beta_{\text{max}} = 1.65$. Larger β -ratios lead to bottom fracture caused by too large bottom forces (Fig. 6b). The strain paths of a drawn cup with a deep drawing ratio $\beta = 1.6$ show that the regions at the punch radius (A-E in Fig. 6c) are deformed along a plane strain path. The regions in the flange and cup wall develop towards the left side of the strain diagram and show a slight nonlinear strain history.

The preliminary numerical investigations of deep drawn solid sheets made from AM 316 L reveal a maximum deep drawing ratio $\beta = 1.65$. This serves as a guideline for the tooling construction that is necessary to be able to deep draw the additively manufactured sheets with a structured core in the upcoming investigations.

Experimental setup

The deep drawing process is conducted on a Zwick/Roell BUP 1000 with a maximum force of 1000 kN. The tools are designed based on machine and design restrictions from previous experiments using the structured sheets [1]. The tool setup is shown in Fig. 7 and is designed to be able to draw solid sheets up to a thickness of $t = 4$ mm with a maximum diameter $d_0 = 250$ mm. A constant blankholder distance of 4.5 mm is used without an additional blankholder force. The friction coefficient was experimentally determined in a strip-drawing test as $\mu = 0.1$.

Fig. 6 a) Drawn cups of a solid sheet (no core structure, thickness $t = 4$ mm) in the numerical simulation using the AM material 316 L, b) Major and minor strains of the drawn cups, c) Strain paths along the outer surface of a drawn cup at specific locations

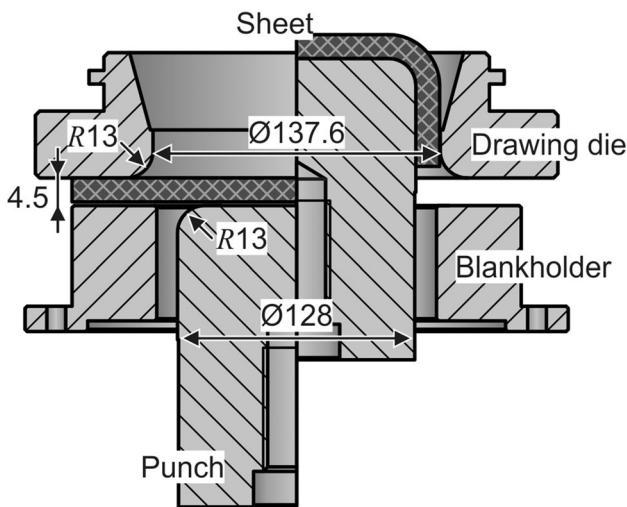
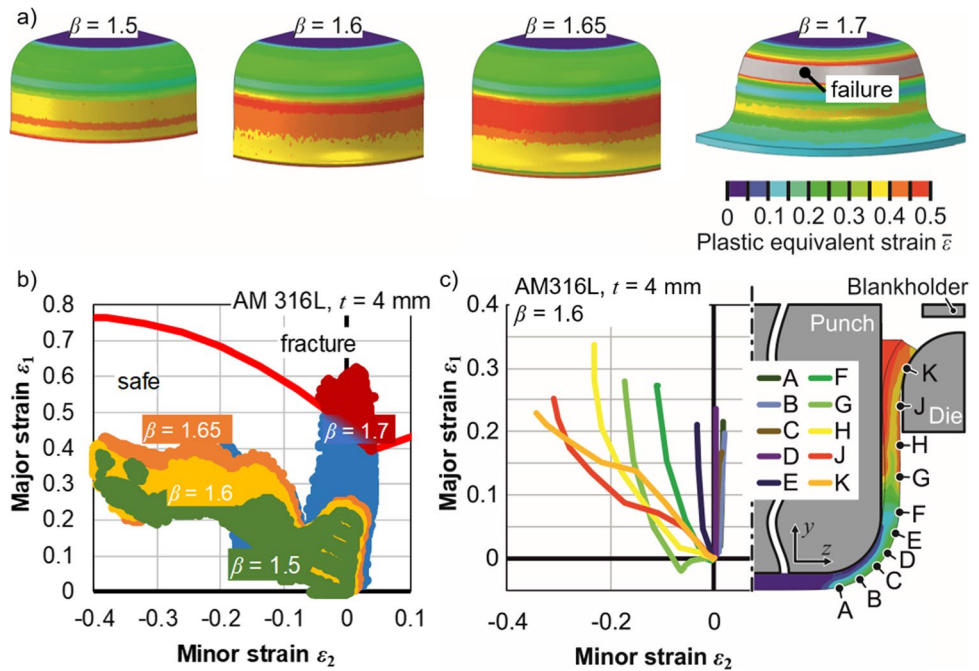


Fig. 7 Tool setup for the deep drawing of the sheets with core structures (dimensions in mm)

Numerical investigations

The numerical investigations are performed using Abaqus CAE 2020 with the explicit solver. The tool is made from rigid shell elements with a mean mesh size of 0.5 mm. The structured sheet is meshed with hexahedral continuum elements (C3D8R-Elements) with a mean mesh element size of 0.25 mm and a global mass-scaling factor of 8. The face sheets are modeled with a minimum of 2 element in thickness direction. The in-plane torsion test flow curve from Fig. 3a is implemented as an isotropic von Mises material

yield criterion without the use of an extrapolation up to a true strain of $\epsilon = 1$. The geometry of the core structure is corrected based on microscopic measurements after the manufacturing of the actual sheets. This revealed chamfers at the corners of the honeycomb structure, as the AM-process cannot produce sharp edges. Although these geometric details are not present in the original CAD-model, they were introduced into the finite element (FEM) model to increase the model accuracy as well as to reduce stress concentrations at sharp corners.

Model setup

Three modeling strategies are tested and compared to evaluate the plastic equivalent strains of deep drawn cups (Fig. 8a). For a better comparability, the strains of the outer face sheet are mapped onto the initially undeformed sheet (Fig. 8b). First, a 30°-model of the deep drawing process (Fig. 8c), second, a 90°-model (Fig. 8d) and third, a 90°-model with a simplified bottom of the drawn cup (Fig. 8e). The computational time for each model is summarized in Table 1.

The visualizations in Fig. 8 show the differences in the modeling approaches. The 30°-model (Fig. 8a) captures the strain distribution in most areas similar to the 90°-model but shows significant differences at the 30°-boundary as a result of the sharp corners where the model is necessarily cut. The stair step-like boundary results from the duplication of the unit cells. A straight cut is not possible since the unit cells are meshed before the duplication to guarantee a good mesh quality. Though the calculation

Fig. 8 Comparison of modeling setups for the numerical simulation of the deep drawing process ($\beta = 1.4$). **a)** Deep drawing process, **b)** Projection of sheet outer surface onto the undeformed geometry, **c)** 30°-model, **b)** 90°-model, **c)** 90°-model with simplified (unstructured solid) cup bottom

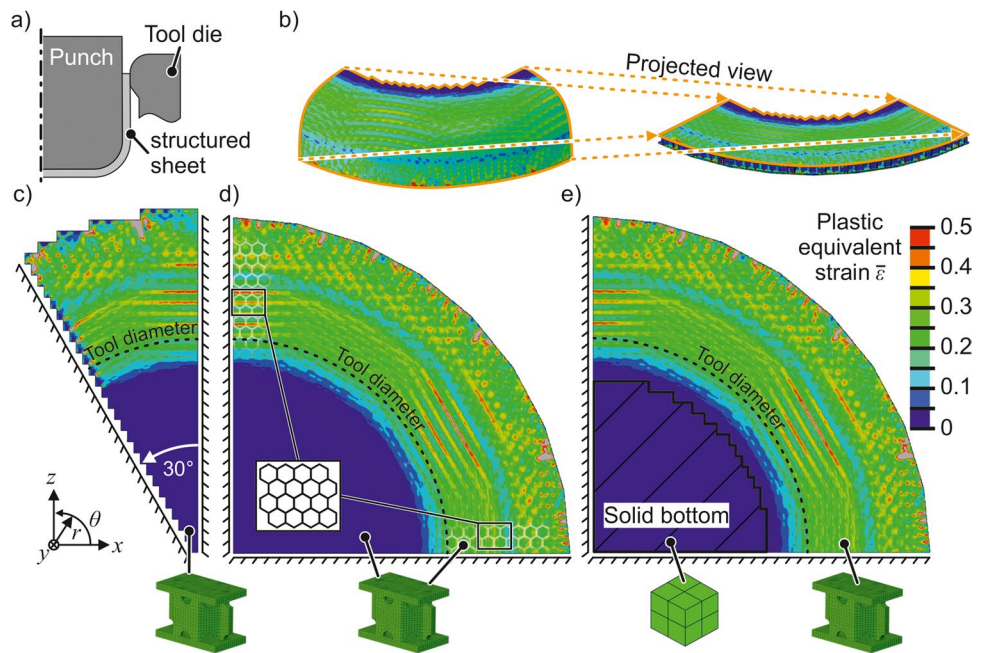


Table 1 Calculation time and number of elements for the different modeling approaches

	30° - model	90° - model	90° - model (simplified cup bottom)
Solving time (8 CPUs*, explicit)	~ 10 h	~ 40 h	~ 20 h
Number of elements	660.000	2.100.000	1.500.000

*Intel Xeon E5-2667 v4 @ 3.2 GHz

time for this model is the lowest across all others (Table 1). Differences between the full 90°-model (Fig. 8b) and the simplified 90°-model (Fig. 8c) are not visible, the strain distribution in the main forming area is equal. No plastic forming takes place under the bottom of the drawing tool, so that the simplification to model this area unstructured with a coarse mesh and it is validated that only elastic behavior occurs. As seen in Fig. 8(b and c), the nature of the core structure leads to a kind of structural and geometrical anisotropy of the part. Strain-wise, it seems like the resultant distribution is recurring twice along the circumference of the 90°-model, i. e. a 45°-model would be the theoretical minimum requirement. Yet, to also avoid the aforementioned boundary problems, the 90°-cut-out is needed to accurately predict all the strains in the whole part during the forming process. The calculation time benefits from the reduced number of elements by a factor of two. Consequently, the accompanying process forces as shown in Fig. 9 can be most accurately predicted by the

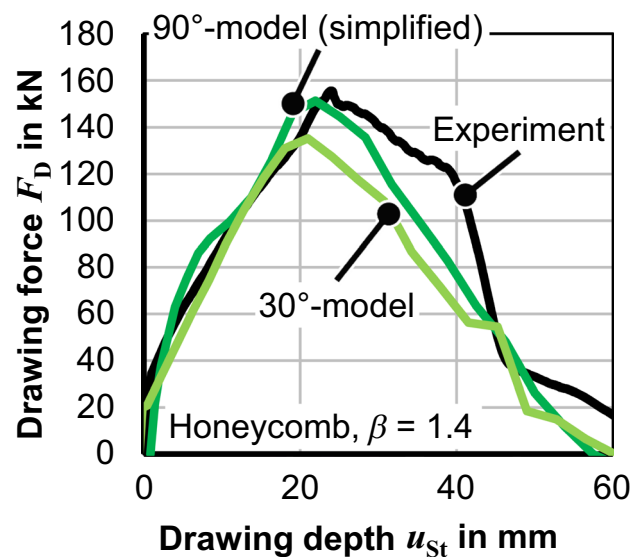


Fig. 9 Deep drawing forces for different modeling approaches

numerical simulation using the 90°-model with the simplified bottom, whereas the 30°-model underestimates the deep drawing forces, especially after the punch displacement (drawing depth) where the peak force occurs. The forces for the 90°-model and 90°-model with the simplified bottom are equal.

Overall, the 90°-model with the simplified bottom offers the most efficient way to predict forces, strains and stresses during the deep drawing process of the structured sheets. Thus, this method is used in the following for a more detailed investigation of the deep drawing process.

Failure analysis in deep drawing

The deep drawing of additively manufactured sheets with a structured core is performed for the deep drawing ratios $\beta = [1.3; 1.4; 1.5]$ (cf. “Preliminary numerical investigations” section). The simulations are evaluated according to the principal strain distribution applying the pre-determined forming limits (Fig. 4a). The results from the deep drawing simulations are shown in Fig. 10. The plastic equivalent strain on the outside of the drawn cup is depicted in Fig. 10a-c. Compared to a conventional drawn cup, the strain distribution is inhomogeneous in radial (r) and tangential (θ) direction. With an increasing drawing ratio β the strains in the face sheet increase and show a unique strain distribution. This unique strain distribution is mainly a consequence of the underlying core structure. It has holes for the powder removal (Fig. 5a) where the core is not fully connected to the face sheet, favoring strain localizations to arise (Fig. 11).

The unsorted final strain map of the fully deep-drawn parts is shown in Fig. 10d-f. The principal strains rise with increasing β and the fracture strain limit is reached for

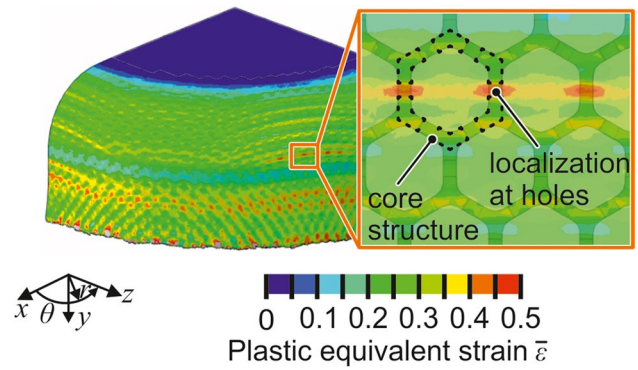


Fig. 11 Strain localization in the face sheet area for $\beta = 1.4$

$\beta = 1.5$ (Fig. 10f), especially in the near-plane strain region, which can be attributed to the bending strains in the area of the tool radius. For deep drawing ratios $\beta < 1.5$ the simulation predicts a successful forming operation.

A closer insight into the strain history offers Fig. 12 at three distinct paths along the radial (r) direction and one

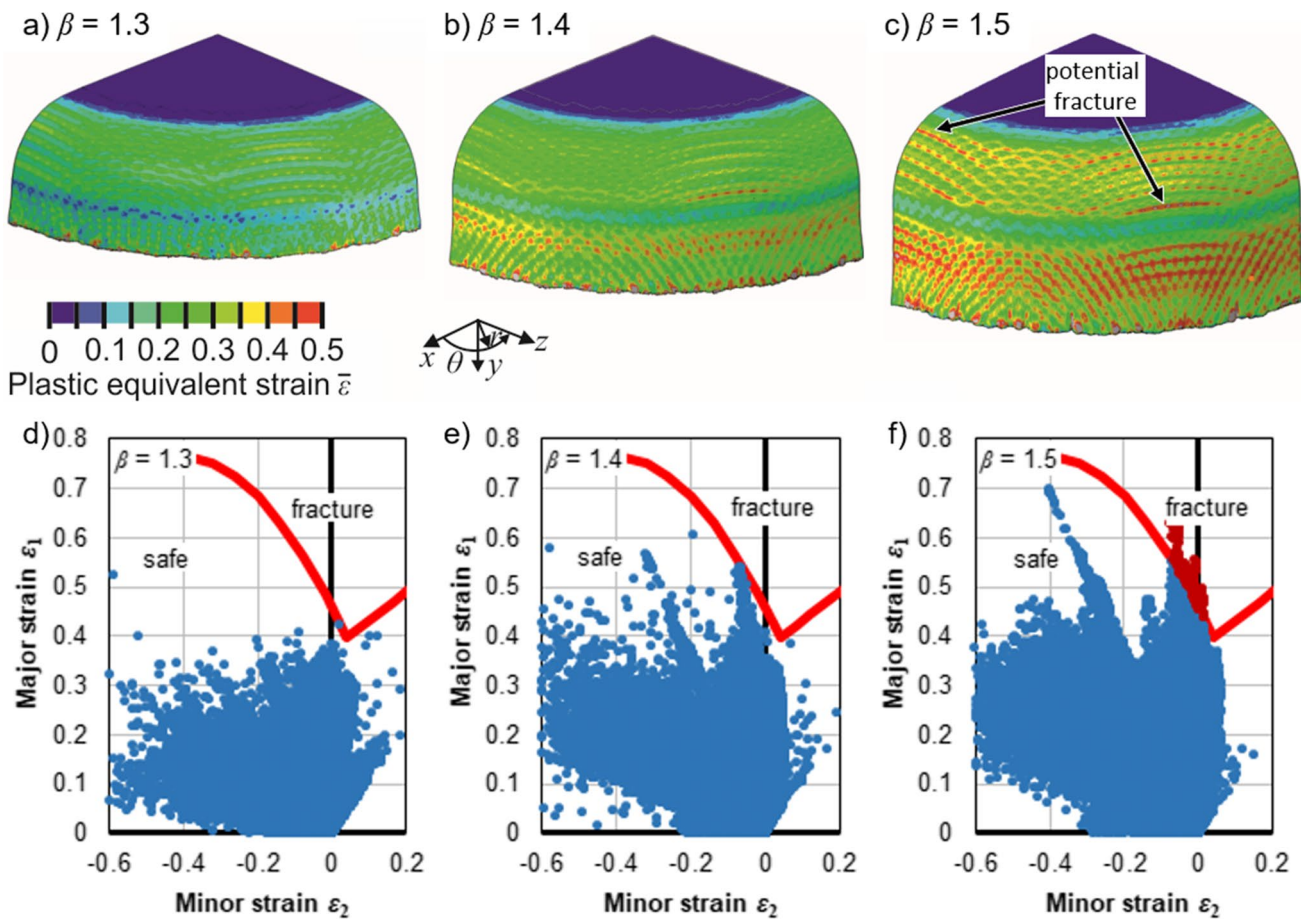
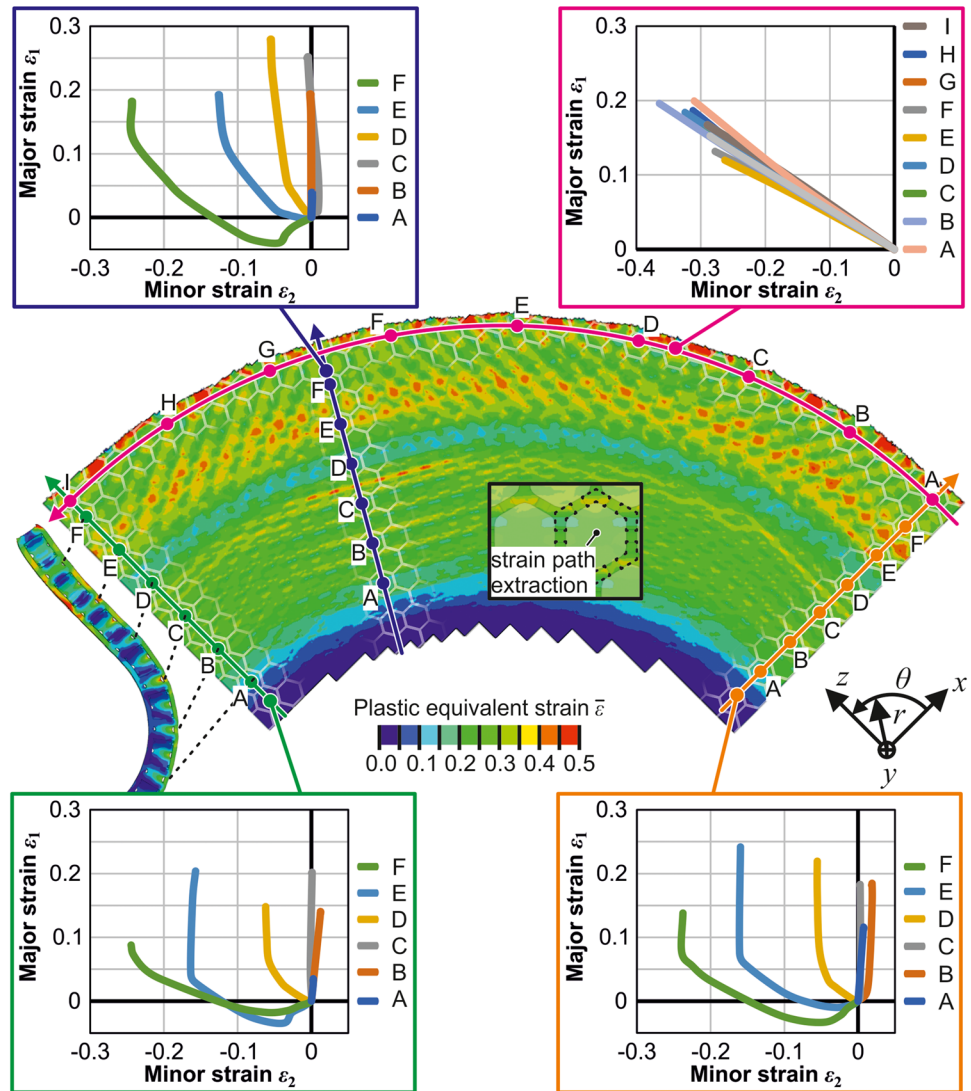


Fig. 10 Results of simulations of the structured sheets for different deep drawing ratios, a-c) Plastic equivalent strain distribution on the outer face sheet, d-f) All major and minor strains existing in the part at the end of the deep drawing simulation

Fig. 12 Strain paths for characteristic points of the drawn cup ($\beta = 1.4$), strains are extracted at the central node inside a unit cell at the outer face sheets



along the meridional (θ) direction. The strain histories are extracted in the center point of a unit cell face sheet. The strain paths in the region of the tool radius, where the dominant forming mechanism is bending, are linear (Fig. 12, radial directions, A – C). In the areas close to the bottom of the cup the reduction of the diameter is small and the face sheet is deformed almost in-plane strain. Investigating the strains further in the radial direction (Fig. 12, radial directions, D – F), the strain paths become more nonlinear and develop towards a biaxial tension-compression deformation. The change of the direction of the strain path starts when the investigated element is drawn into the die after the forming radius, since the reduction of the radius is finished, the tension in drawing direction is dominant. The outer region of the sheet, the flange area, is deformed linearly during the whole deep drawing process in the typical tension-compression deformation all over the meridional direction (Fig. 12, pink A – I). Comparing the strain paths

for the three investigated radial directions (Fig. 12, purple, green, orange), it can be seen that the strain history is almost independent of the investigated angle in the radial direction. Differences arise in the amplitude of the strains as a result of the underlying geometrical anisotropy of the core structure.

A comparison between the strain history of a solid and a structured deep drawn cup, both $\beta = 1.4$, gives Fig. 13. The investigated locations for the strain history are equal for the solid and the structured sheet and equal to the locations discussed in Fig. 12. The strain paths of the locations that are mainly deformed as a result of bending (Fig. 14A-D) have almost the same strain history. Differences arise in the amplitude, thus the amount of induced deformation is larger for the structured sheet. This results from the localization of the deformation in the face sheets, since the core does not offer a homogeneous support for the face sheets. The largest differences can be seen in location F. After the compression in radial and meridional direction the load is concentrated

Fig. 13 Strain path comparison of solid and structured sheets

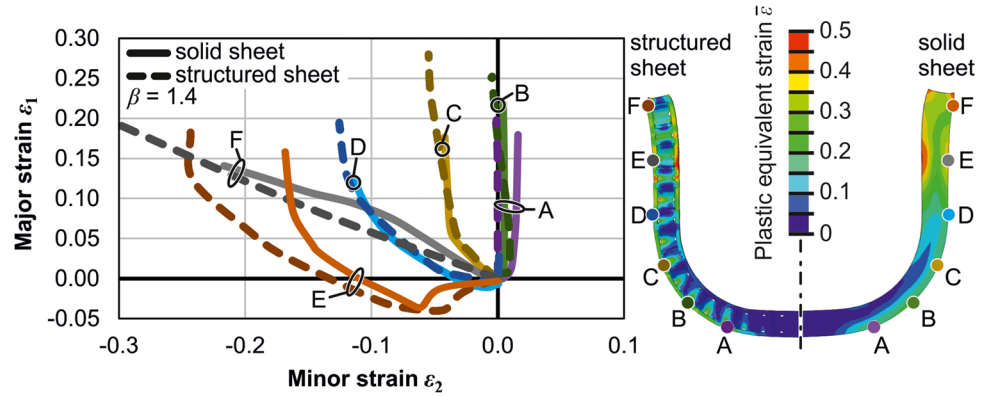
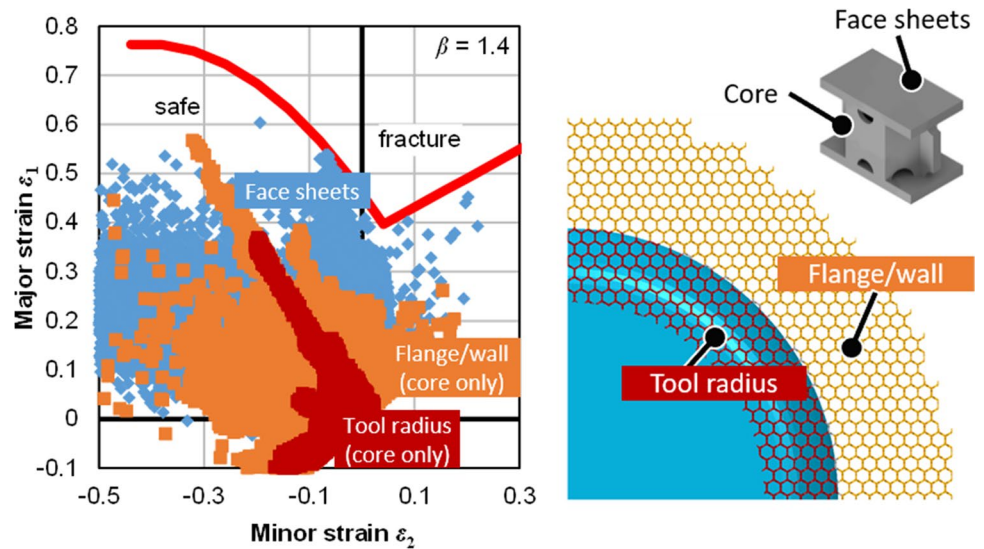


Fig. 14 Separated final strain map of the deep-drawn honeycomb cup including failure limits



in the face sheets leading to larger strains. Qualitatively the shapes of the strain paths are the same. The differences in the strain paths are mainly visible in the amplitude of the strains. This leads to the conclusion that the core structure may not significantly influence the strain paths of the sheets, as long as the core structure stays intact, but the strain amplitude is influenced. This needs to be further investigated in future studies.

A more separated insight into the strain map of the structured sheet gives Fig. 14. The strains are plotted separately for the core itself, for the area of the core underneath the tool radius, and the flange area which is drawn into the die. Next to that, the strains of the face sheets are displayed separately as well. The strains of the core structure are mainly located in the strain area related to shearing. In comparison, the face sheet data relates to all occurring strain pairs. It is, however, noticeable that the points which become critical are only located in the face sheet and not in the core structure.

A key advantage of numerical computations is that experimentally not accessible spaces can be analyzed. So,

the drawn cup ($\beta = 1.4$) with hidden face sheets, viz. the deformed core structure, can be seen in Fig. 15a from three perspectives. Severe deformation, like buckling of the cell walls or excessive distortion is not visible. The core structure forms a relatively even shape in the deep drawing process. A detailed history plot of the deformation of the core structure at four distinct locations shows Fig. 15c, the locations are marked in Fig. 15b. A closer look at the deformation state reveals two main characteristics. The cell in location A deforms almost in the same way as the cell in location C, and the same applies to the cells in the locations B and D after rotating the structure into the same orientation (Fig. 16). The deformation of the structure solely depends on its location in the meridional (θ) direction. Since the deformation can be attributed to two main directions, a characterization of the unit cells in two directions appears adequate. Another previously stated fact can be proved from the periodicity of the observed core deformation: All the information about the deformation characteristics is included in a 45° -portion of the model. From there, the deformation of the core repeats in a rotationally periodic manner.

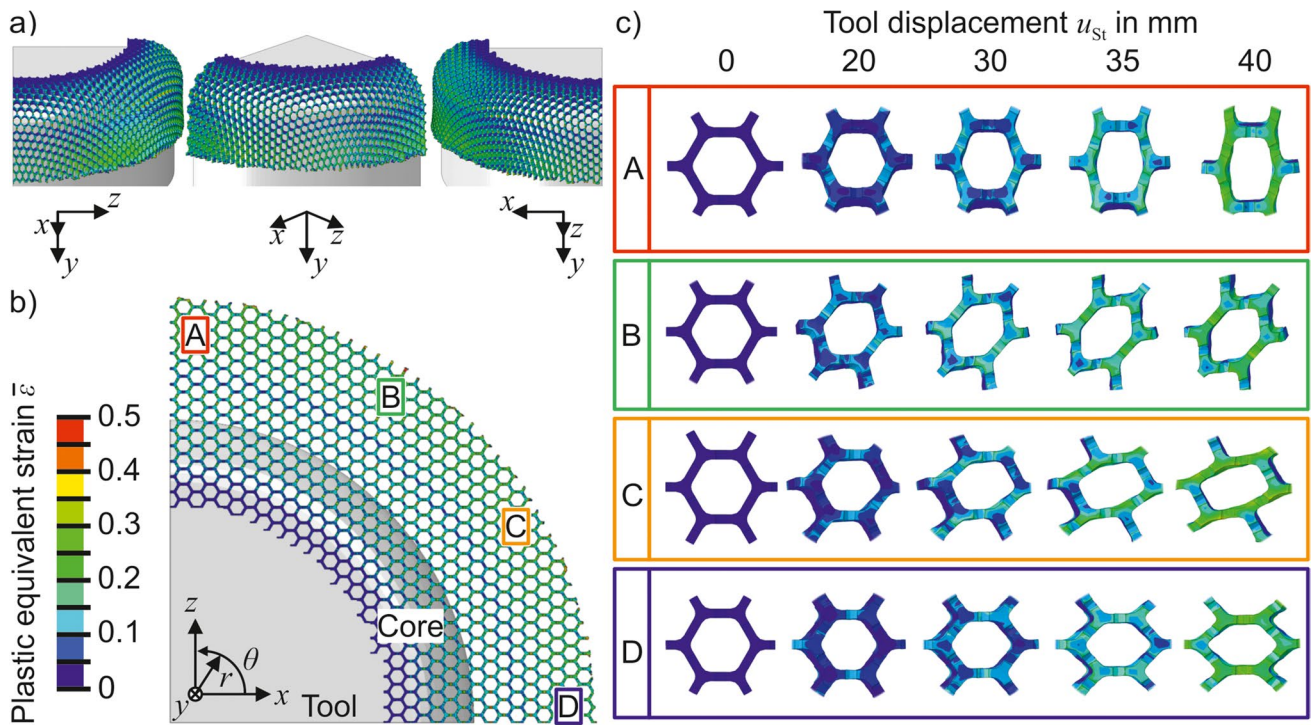


Fig. 15 Plastic deformation of the core structure for $\beta=1.4$, **a)** Isometric views of the drawn cup with hidden face sheets, **b)** Projected view of the core structure, **c)** Deformation history of unit cells at different locations

Expanding the investigations to core structures with varied relative density ρ_{core} , the reached strains of the correspondingly drawn cups are compiled in Fig. 17. With increasing density ρ_{core} the strains increase in their absolute values. Failures due to large strains occur again for deep drawing ratios $\beta > 1.5$.

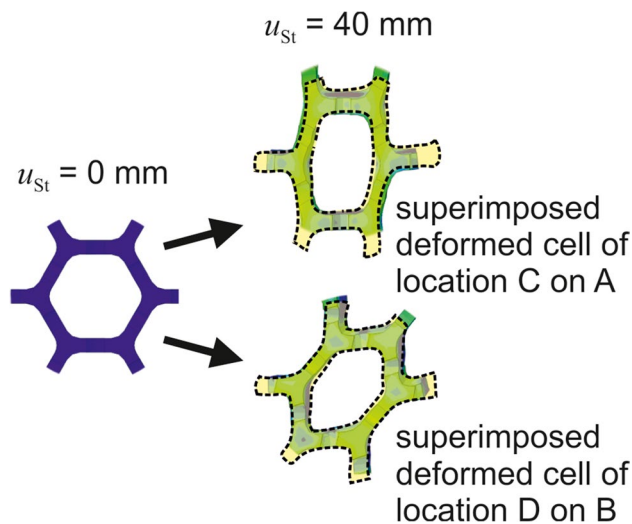


Fig. 16 Deformation shape of core structure cells with superimposed deformed cells of the locations from Fig. 15. (drawing depth u_{St})

The increasing strains with rising relative density ρ_{core} and deep drawing ratio β are depicted in Fig. 18. Reduced relative densities lead to fewer strain concentrations in the area of the face sheets where they are not connected to the core. This phenomenon can be attributed to the fact that the internal distance between the core cell walls diminishes with increasing relative density. Therefore, the strains during the forming operation are distributed or concentrated over a smaller area, which eventually results in larger local strains.

The failure of the cup with a low density-core of $\rho=0.1$ during the deep drawing operation is visible in Fig. 19 as a result of a series of different developments. During the forming of the cup, the sheet is drawn into the die, which forces the flange into a compressive stress state in the meridional (θ) direction. Before the forming in meridional direction begins, the sheet is pushed by the punch and reacts with an upward-movement at the outer flange area and is pushed against the blank holder. The resulting stresses in thickness direction lead to an initial imperfection in the outer walls of the core structure (Fig. 19a). The subsequent forming in meridional direction leads to compressive stresses that then lead to a plastic buckling of the face sheets because of the reduced stiffness of the core (Fig. 19b). This initial imperfection develops further to a global buckling phenomenon of the whole structure in the outer area of the flange (Fig. 19c).

The numerical investigations show that the use of semi-finished sheets with a core structure in a deep drawing

Fig. 17 All major and minor strains at the end of the deep drawing process for a variation of the relative density $\rho_{core} = [0.1; 0.22; 0.32]$ and deep drawing ratios $\beta = [1.3; 1.4; 1.5]$

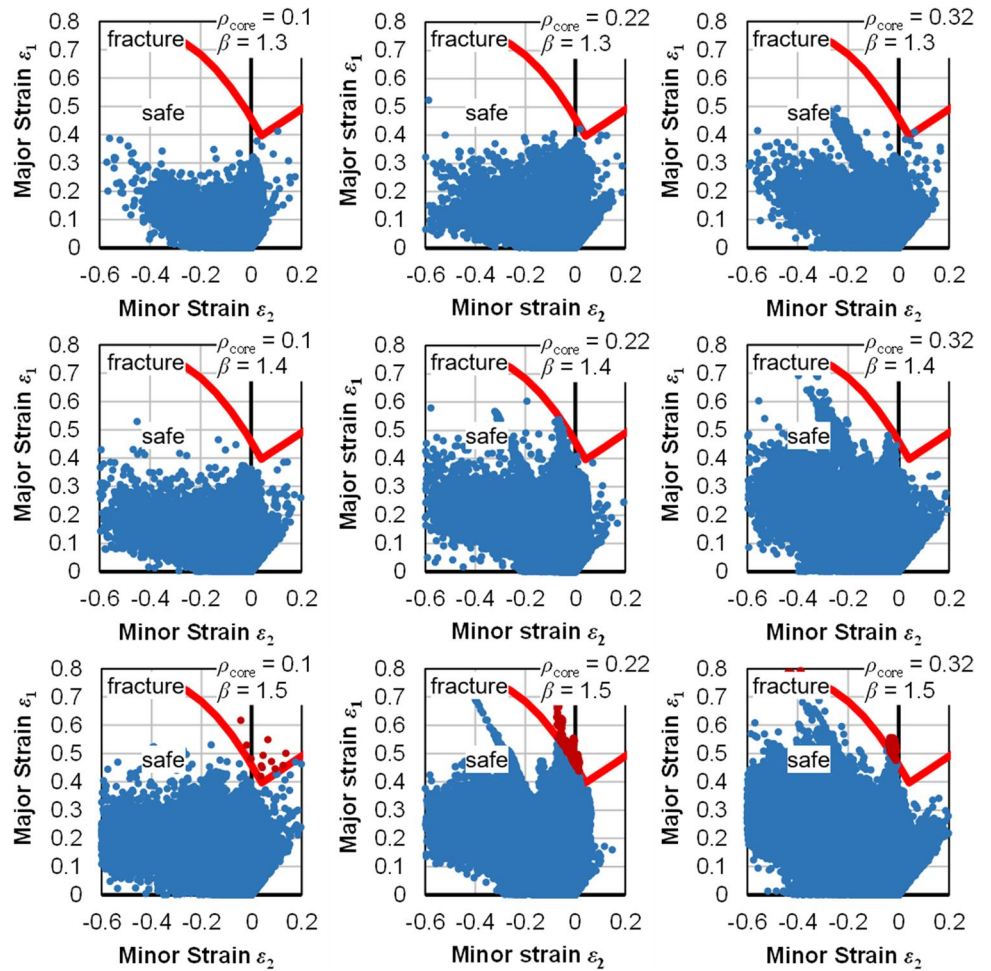
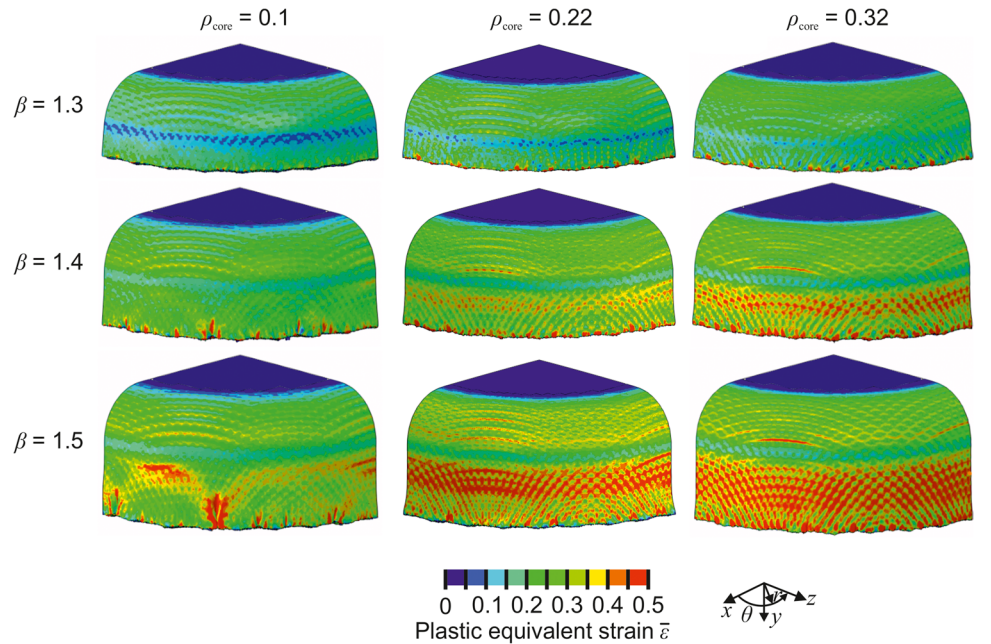


Fig. 18 Plastic equivalent strains $\bar{\epsilon}$ for varied relative densities ρ_{core} and deep drawing ratios β at the outer face sheet



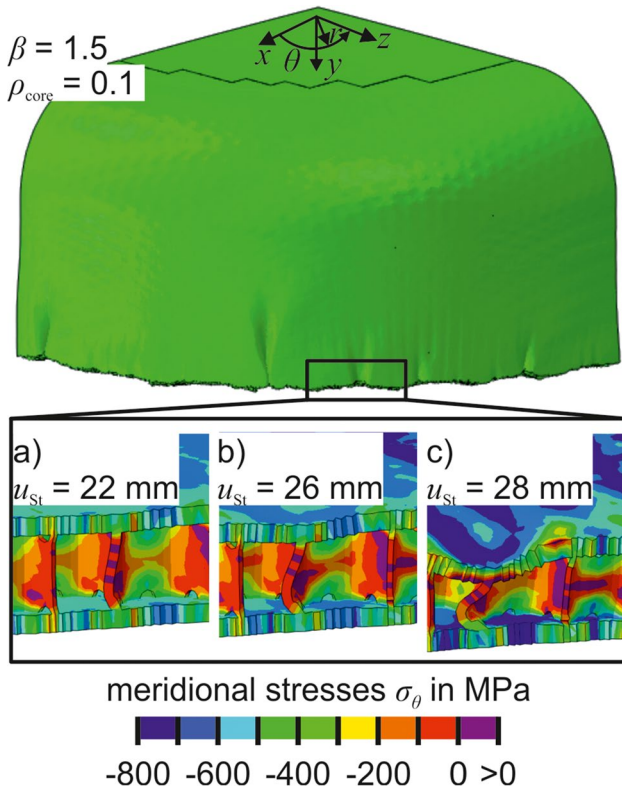


Fig. 19 Possible failure mode of the core structure during deep drawing, a) – c) Show different drawing depth u_{St}

process can be expected to be feasible. Process limitations and failure modes were identified, together with key deformation characteristics. In the following section, the simulations are validated experimentally.

Experimental investigation

The numerical results of the previous section are validated by deep drawing semi-finished sheets with a relative core density $\rho_{core} = 0.22$ and face sheet thickness $t_f = 0.5$ mm (recall Fig. 5). The tool design was already explained in Fig. 7.

The resultant cups of the deep drawing experiments are shown in Fig. 21. Different deep drawing ratios β are addressed. The experiments were successful for values of $\beta \leq 1.4$ (Fig. 21a, b). These drawn cups do not show failure of the face sheets or failure of the core structure. The outer

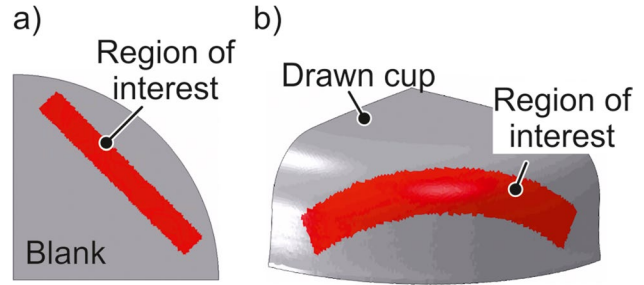


Fig. 20 a) Blank before deepdrawing, b) Deformed region of interest in the drawn cup

area of the flange shows signs of local wrinkling of the face sheets at the laser cutting edge. This is due to a reduced stiffness of the face sheets because the cells of the core are not closed at these edges. Therefore, the face sheets can wrinkle into these open cells of the core (Fig. 21b). For the regions where the cells of the core structure are fully closed, such failure is not present.

Deep drawing ratios $\beta \geq 1.5$ show severe damage of the cup. The face sheets fail under the forming loads and cracks in the characteristic arc shape develop. The arc shape is not exclusively related to deep drawing of structured sheets but gets visible due to the inhomogeneous material distribution of the core. As seen in Fig. 20 rectangular portions are deformed into such arc shapes. The marked crack in Fig. 21c is the first crack. Afterwards, another crack developed and ripped the whole wall of the cup apart. The location of this failure was predicted by the previous numerical simulation.

The corresponding force-displacement diagrams are depicted in Fig. 22, comparing the numerically predicted process forces with the experiments. Their overall agreement can be termed good. The mean deviation between simulation and experiment is 13%. For a simple comparative prediction of the process forces, it is also checked if the calculation according to Siebel [10] can be used. The formulae is based on the balance of power and calculate the maximum deep drawing force $F_{Max, Siebel}$ in Eq. (1). To make Siebel's equation applicable to the forming of the structured sheets it is assumed that the structured sheet behaves like a solid sheet but with a reduced stiffness. That means that the predicted forces for the considered deep drawing process are simply multiplied with the relative density ρ_{sheet} of the structured sheet.

$$F_{Max, Siebel} = \pi d_m H \left[e^{\mu\alpha} \left(1.1\sigma_{fm,1} \ln \frac{D}{d_m} + \frac{2\mu F_{BH}}{\pi DH} \right) + \sigma_{fm,2} \frac{H}{2r_d} \right] \cdot \rho_{sheet} \tag{1}$$

Fig. 21 Deep-drawn cups of additively manufactured sheets with core structures for a relative density of $\rho_{\text{core}} = 0.22$, and drawing ratios of **a)** $\beta = 1.3$, **b)** $\beta = 1.4$, **c)** $\beta = 1.5$

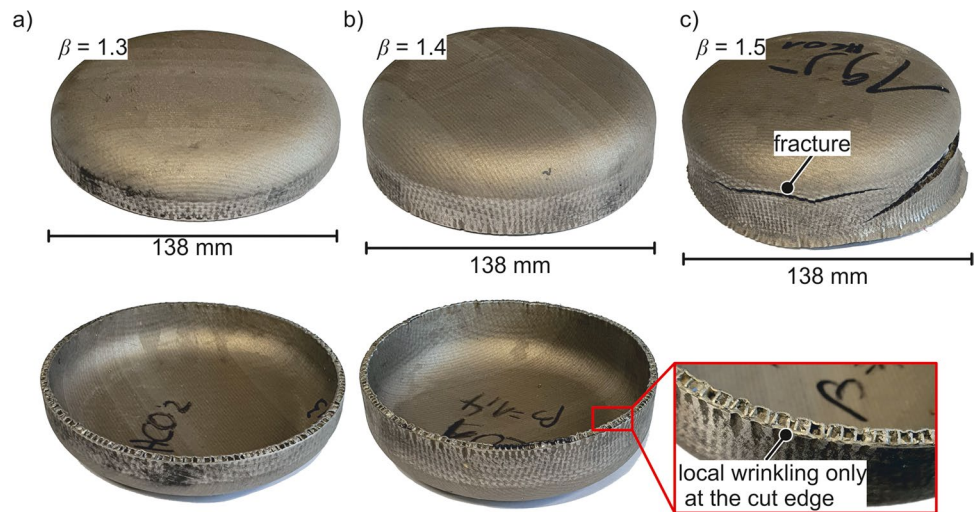
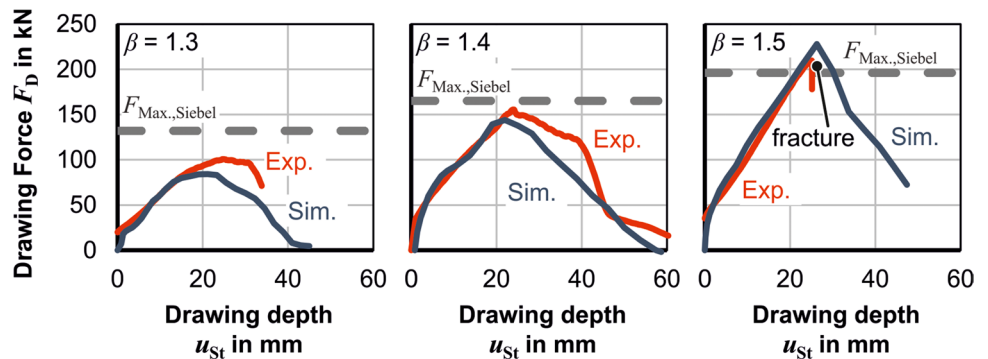


Fig. 22 Deep drawing forces for the drawn cups for the three chosen drawing ratios



where d_m is the mean cup diameter, D is the flange diameter when the maximum force occurs, H is the overall sheet thickness, $\sigma_{\text{fm},1}$ is the average flow stress corresponding to the strain from the outer radius to the inner radius of the flange, $\sigma_{\text{fm},2}$ is the average flow stress before and after the bending of the metal sheet at the die radius, α is the die radius angle, r_d the die radius and F_{BH} the blankholder force.

This leads to a reasonable approximation of the maximum process forces as seen in Fig. 22.

Process window

The results of the previous investigations can be summarized in a process window diagram that can be seen in Fig. 23. The diagram shows possible combinations of the relative density of the honeycomb core structure and the deep drawing ratio. The main failure modes that can occur are fracture of the face sheets or global buckling of the structured sheet. Although this process window here applies for a specific AM-material and core geometry, it is inferred that the general failure modes and qualitative appearance of the deduced window are representative for other such combinations as well.

Conclusion and outlook

The presented research focused on the investigation of the deep drawability of additively manufactured semi-finished sheets with a structured core. The lightweight core structure serves the purpose of an innovative lightweight part with a high stiffness. The proposed structured sheets benefit from the design freedom of the additive manufacturing process and can be used to tailor the sheet or to further integrate functions. The approach of subsequently forming the flat sheets, instead of directly printing the final product, has the main advantage of an overall increased process efficiency.

The presented work shows that the deep drawing into cups is possible with those additively manufactured structured sheets, and the following conclusions can be drawn:

- Deep drawing of additively manufactured semi-finished sheets is possible with a maximum deep drawing ratio of $\beta_{\text{max}} = 1.4$ and a relative core density $\rho_{\text{core}} = 0.22$. This is lower compared to deep drawing a solid sheet using the same process parameters reaching $\beta_{\text{max}} = 1.65$. Severe deformation of the core structure did not occur and the

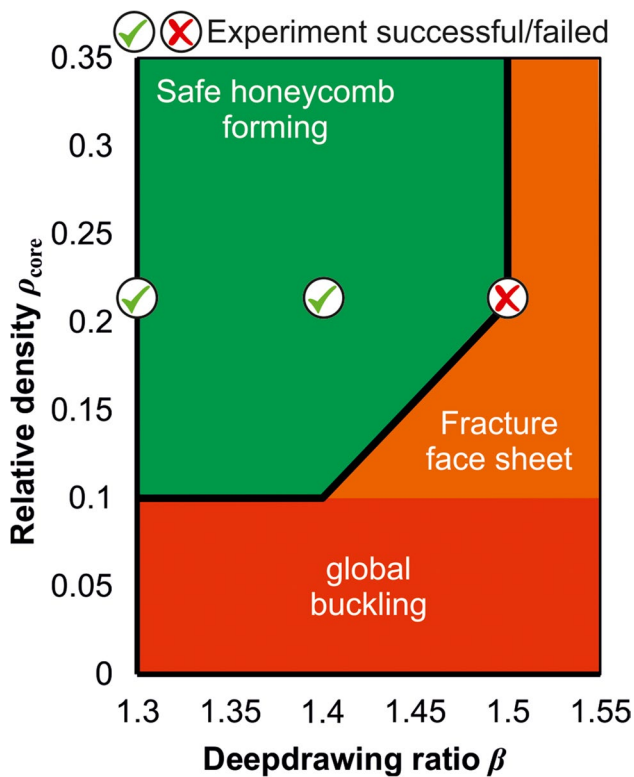


Fig. 23 Process window for deep drawing of structured sheets with a honeycomb core

structural integrity of the core was kept in the final part. Small relative core densities $\rho_{\text{core}} = 0.1$ lead to global buckling in the flange area but a more homogeneous strain distribution in the face sheets.

- The overall formability is mainly determined by the face sheets, as long as the structural integrity of the core stays intact. The strain path history of the structured sheets is almost the same as for solid sheets but with the structured sheets exhibiting larger strains due to strain localizations in the face sheets. Thus the classical deep drawing knowledge can be used to analyze the process.
- The strains in the face sheets are influenced by the transition zone between the face sheets and the core, which should be homogeneous without additional discontinuities. Shifting the powder holes to remove the excess powder of the AM process to the centerline of the core potentially increases the formability of the face sheets due to less strain concentrations. However, this results in a significantly harder removal of the remaining powder due to undercuts. The explicit design of the core seems to be of secondary importance but will be further investigated.
- The investigations show that the deep drawn cup during forming is loaded to different extents at various locations, e. g. the bottom is only loaded elastically. Therefore a tailoring of the core structure by means of grading the

core and wall thicknesses could lead to a further increase of the lightweighting – assuming that the requirements for the subsequent load case remain fulfilled. The trade-off between good formability vs. lightweight design vs. subsequent application is challenging.

The forming of additively manufactured semi-finished sheets is an alternative approach for producing sheet parts with a lightweight core structure. Future research will investigate the forming characteristics of other core structures and the possibility of using topology optimization to generate advantageous core structures that are otherwise not manufacturable conventionally. Also, a hybrid approach is planned where only the complex core structure is additively manufactured and the face sheets are joined to it, allowing to overcome the build chamber volume restrictions of current additive manufacturing machines.

Acknowledgements This paper is based on results of the project ‘Forming of additively manufactured sandwich sheets with optimized core structures’ (Project number 317137194), which is kindly supported by the German Research Foundation (DFG). The authors would also like to thank Mike Kamaliev, Joshua Grodotzki, Dirk Hoffmann and Werner Feurer for their input.

Funding Open Access funding enabled and organized by Projekt DEAL.

Declarations

Conflict of interest The authors have no conflict of interest.

Open Access This article is licensed under a Creative Commons Attribution 4.0 International License, which permits use, sharing, adaptation, distribution and reproduction in any medium or format, as long as you give appropriate credit to the original author(s) and the source, provide a link to the Creative Commons licence, and indicate if changes were made. The images or other third party material in this article are included in the article's Creative Commons licence, unless indicated otherwise in a credit line to the material. If material is not included in the article's Creative Commons licence and your intended use is not permitted by statutory regulation or exceeds the permitted use, you will need to obtain permission directly from the copyright holder. To view a copy of this licence, visit <http://creativecommons.org/licenses/by/4.0/>.

References

1. Rosenthal S, Hahn M, Tekkaya AE, Platt S, Kleszczynski S, Witt G (2021) Speeding up additive manufacturing by means of forming for sheet components with Core structures. *Int J Precis Eng Manuf-Green Tech.* <https://doi.org/10.1007/s40684-021-00384-x>
2. Cai Z-Y, Liang X-B, Chen Q-M, Zhang X (2018) Numerical and experimental investigations on the formability of three-dimensional aluminum alloy sandwich panels with egg-box-like cores. *Int J Adv Manuf Technol* 4. <https://doi.org/10.1007/s00170-018-2499-3>
3. Cai Z-Y, Zhang X, Liang X-B (2018) Multi-point forming of sandwich panels with egg-box-like cores and failure behaviors in forming process: analytical models, numerical and experimental investigations. *Mater Des.* <https://doi.org/10.1016/j.matdes.2018.10.037>

4. Liang X-B, Cai Z-Y, Zhang X, Gao J-X (2020) Plastic forming of the doubly curved surfaces of sandwich plates with bi-directionally trapezoidal cores of different sizes. *Thin-Walled Struct.* <https://doi.org/10.1016/j.tws.2019.106188>
5. Seong DY, Jung CG, Yang DY, Kim JH, Chung WJ, Lee MY (2010) Bendable metallic sandwich plates with a sheared dimple core. *Scr Mater* 1. <https://doi.org/10.1016/j.scriptamat.2010.03.022>
6. Seong DY, Jung CG, Yang DY, Ahn J, Na SJ, Chung WJ, Kim JH (2010) Analysis of core shear stress in welded deformable sandwich plates to prevent de-bonding failure during U-bending. *J Mater Process Technol* 9. <https://doi.org/10.1016/j.jmatprotec.2010.02.026>
7. Traphöner H, Clausmeyer T, Tekkaya AE (2018) Material characterization for plane and curved sheets using the in-plane torsion test – an overview. *J Mater Process Technol* 1. <https://doi.org/10.1016/j.jmatprotec.2018.02.030>
8. (2009) *Metallic materials - Sheet and strip - Determination of forming-limit curves - Part 2: Determination of forming-limit curves in the laboratory*((ISO 12004-2:2008))
9. Saunders N, Miodownik AP (2005) *CALPHAD calculation of phase diagrams. A comprehensive guide.* Pergamon materials series, vol. 1. Pergamon, Oxford
10. Siebel E, Beisswänger H (1955) *Tiefziehen: Forschungsarbeiten auf dem Gebiete des Tiefziehens im Auftrage der Forschungsgesellschaft Blechverarbeitung.* Hanser-Verlag, München

Publisher's note Springer Nature remains neutral with regard to jurisdictional claims in published maps and institutional affiliations.